Spring 2023

CE-QUAL-W2 Performance Assessment Modeling 1979 GRH Flume Study

Logan Negherbon
Portland State University

CE-QUAL-W2 Performance Assessment Modeling 1979 GRH Flume Study

BY

Logan Negherbon

A research project report submitted in partial fulfillment
of the requirement for the degree of

MASTER OF SCIENCE
IN
CIVIL AND ENVIRONMENTAL ENGINEERING

Project Advisor:
Dr. Scott A. Wells

Portland State University

ACKNOWLEDGMENTS

I would like to express the greatest appreciation for my advisor and professor, Dr. Scott Wells, who has guided me through the research present here.

I would also like to acknowledge my wife, Marya Choudhry, who supported and encouraged me throughout the course of my graduate studies and especially these last months as we expect our first child.

ABSTRACT

In an early review of numerical reservoir hydrodynamic models, the US Army Corps of Engineers developed a physical model at the US Army Waterways Experiment Station to assess the performance of modeling cold water underflow with numerous 2-dimensional and 3-dimensional numerical hydrodynamic models. Within this effort, the precursor for CE-QUAL-W2, the Laterally Averaged Reservoir Model, was defined and applied with limited success in representing the vertical velocity profile and outflow temperatures series collected from the physical model in the General Reservoir Hydrodynamics flume. CE-QUAL-W2 has since been modified from this early form in numerous ways including incorporation of higher order transport schemes, additional vertical turbulence algorithms and implicit solutions for effects of vertical eddy viscosity to note only a few of the hydrodynamic optimizations. Among these modifications, model has undergone many other rewrites and additions to address emerging applications and higher order water quality constituent models that will not be addressed within this assessment. This research project investigates the performance of the current version (v4.5) of CE-QUAL-W2 in matching the experimental results from presented within the Technical Report documenting the physical study and model review.

TABLE OF CONTENTS

LIST OF TABLES

LIST OF FIGURES

1.0 INTRODUCTION

1.1 Background

CE-QUAL-W2

CE-QUAL-W2 is a two-dimensional laterally averaged hydrodynamic model used broadly for modeling time-varying water quality within rivers, lakes, reservoirs, estuaries and any combination thereof. The model originated as the Laterally Averaged Reservoir Model (LARM) in 1975 developed by Edinger and Buchak and through subsequent iterations resulted in CE-QUAL-W2 Version 1.0 which itself has been developed to Version 4.5. Although not unique to this latest update, Version 4.5 include numerous improvements to the underlying code and user inputs capabilities. Among them are the turbulent closure algorithms, numerical transports schemes and implicit numerical solutions (Wells, 2023).

In this study, the performance of CE-QUAL-W2 was assessed with various spatial resolutions and input parameters against set of physical model data developed to support density stratified flow modeling of reservoirs.

GRH Flume Experiment and Data

The U.S. Army Corps of Engineers conducted a study of numerical reservoir models, Technical Report E-81-2, in 1978 to 1980 with the objective of recommending a tool for predicting reservoir hydrodynamics and subsequently water quality parameters over extended periods of time. The study assessed numerous two-dimensional and three-dimensional, unsteady, variable density models with thermal transfer capabilities. The General Reservoir Hydrodynamics (GRH) flume located at the U.S. Army Engineer Waterways Experiments Station (WES) was used as a physical benchmark for the models' performance (Johnson 1981). The GRH flume is constructed of clear plastic to facilitate visualization of flow patterns. The GRH flume was house in a climate-controlled room and had inflow control for temperature and volume (Dortch 1985).

The GRH flume modeling domain was 24.39 meters in length with an upstream boundary cross section of 0.30 meters wide by 0.30 meters deep. From the upstream boundary section, the flume channel laterally expanded by 0.61 meters over a distance for 6.10 meters with no change

in floor slope to an intermediate section 0.91 meters wide by 0.30 meters deep. From this intermediate section, the flume channel floor descended 0.61 meters at a constant slope over the remaining 18.29 meters for a termination section of 0.91 meters wide by 0.91 meters deep. Inflow entered 0.46 meters upstream of the flume boundary section where a solid panel baffle descended 0.15 meters into the flow restricting inflow to the lower half of the channel. Outflow exited the downstream termination section from a 0.0254-meter diameter port located 0.15 meters above the floor on the centerline of the flume. The flume water was left at rest to achieve a homogeneous temperature of 70.6 degrees Fahrenheit (21.44 degrees Centigrade) for the initial condition. Upon start of the experiment, cold water inflow then entered the model at 62.0 degrees Fahrenheit (16.67 degrees Centigrade) at a flow rate of 0.00063 cubic meters per second and outflow was with exited the downstream port at the same rate (Johnson 1981).

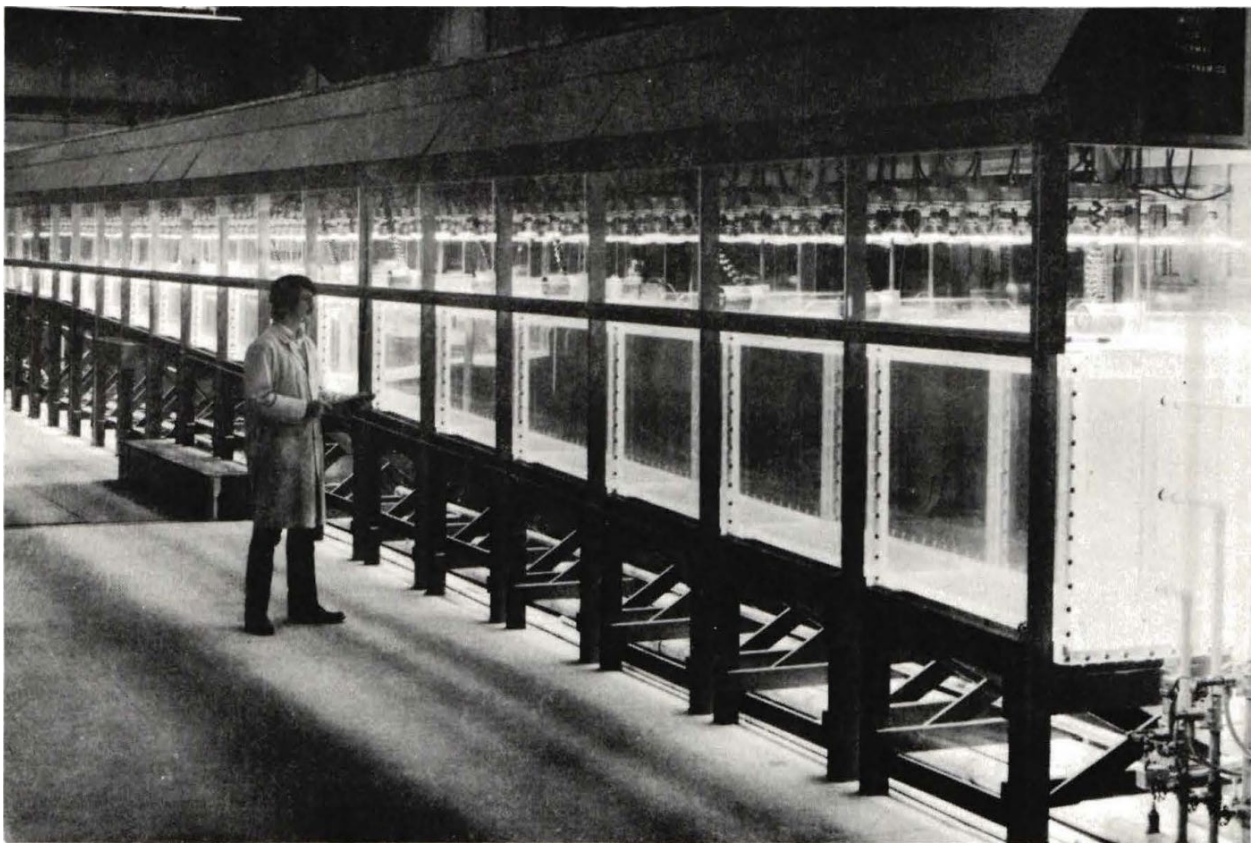

Figure 1: Image of GRH flume looking from downstream end (right) to upstream end (left) with unidentified observer taking notes.

The study recorded data in the form of a temperature time series from the outflow port and a velocity profile at a station 11.43 meters downstream from the upstream flume end. Cold

water inflow was dyed to support visual observation as the density underflow progressed through the flume and the position of the leading edge was position was also documented. Dye streaks shown in Figure 2 were used to observe the velocity profile reported in Figure 2. Visual observations indicated relatively smooth flow likely in the laminar flow range. Examination of the underflow height 7.5 cm and average velocity of 0.022 meters per second (average over the full flume length) with a molecular viscosity of 1.5E-6 m^2/s indicated flow is likely transitional (Johnson 1981).

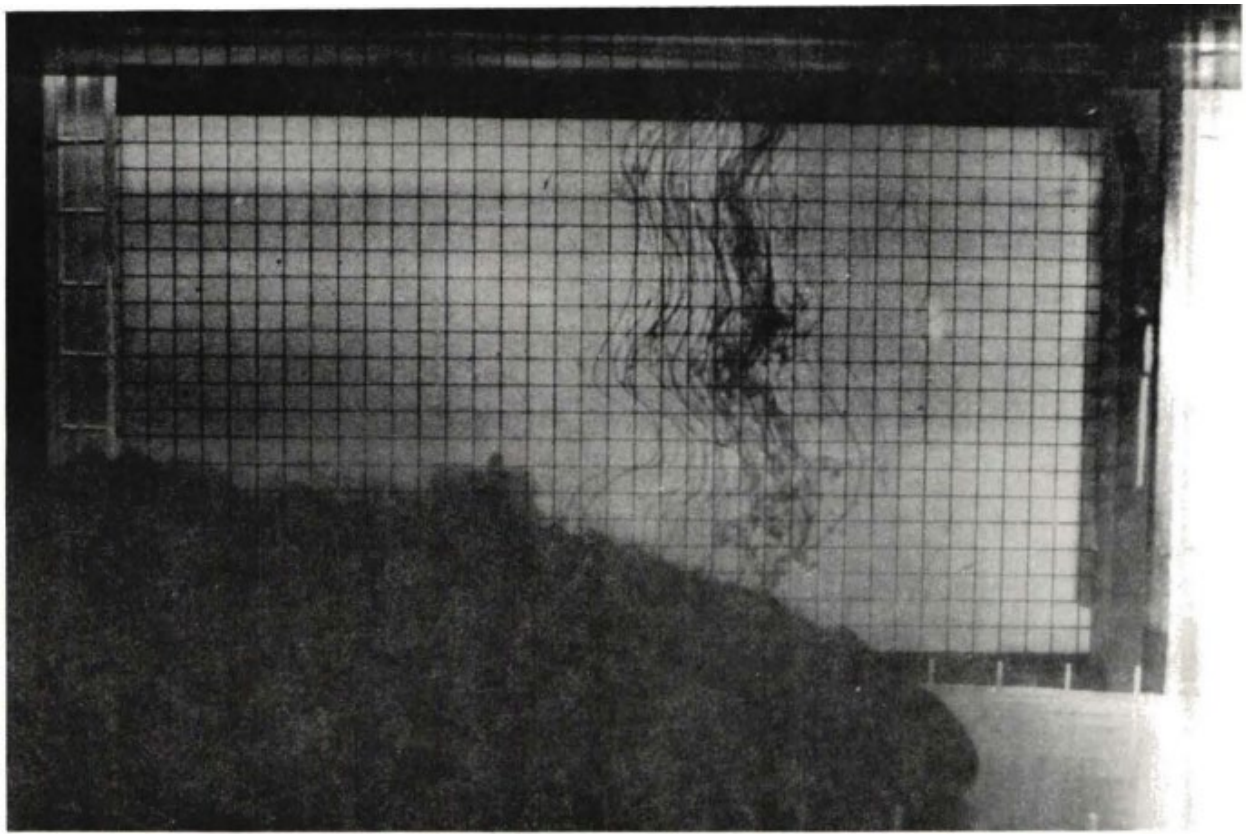

Figure 2: Image of dye streak and dyed density underflow used for data collection (Johnson 1981).

Data presented in graphical form within Technical Report E-81-2 was digitized for model comparison and rendered to the figures (Figure 3, Figure 4 and Figure 5) below.

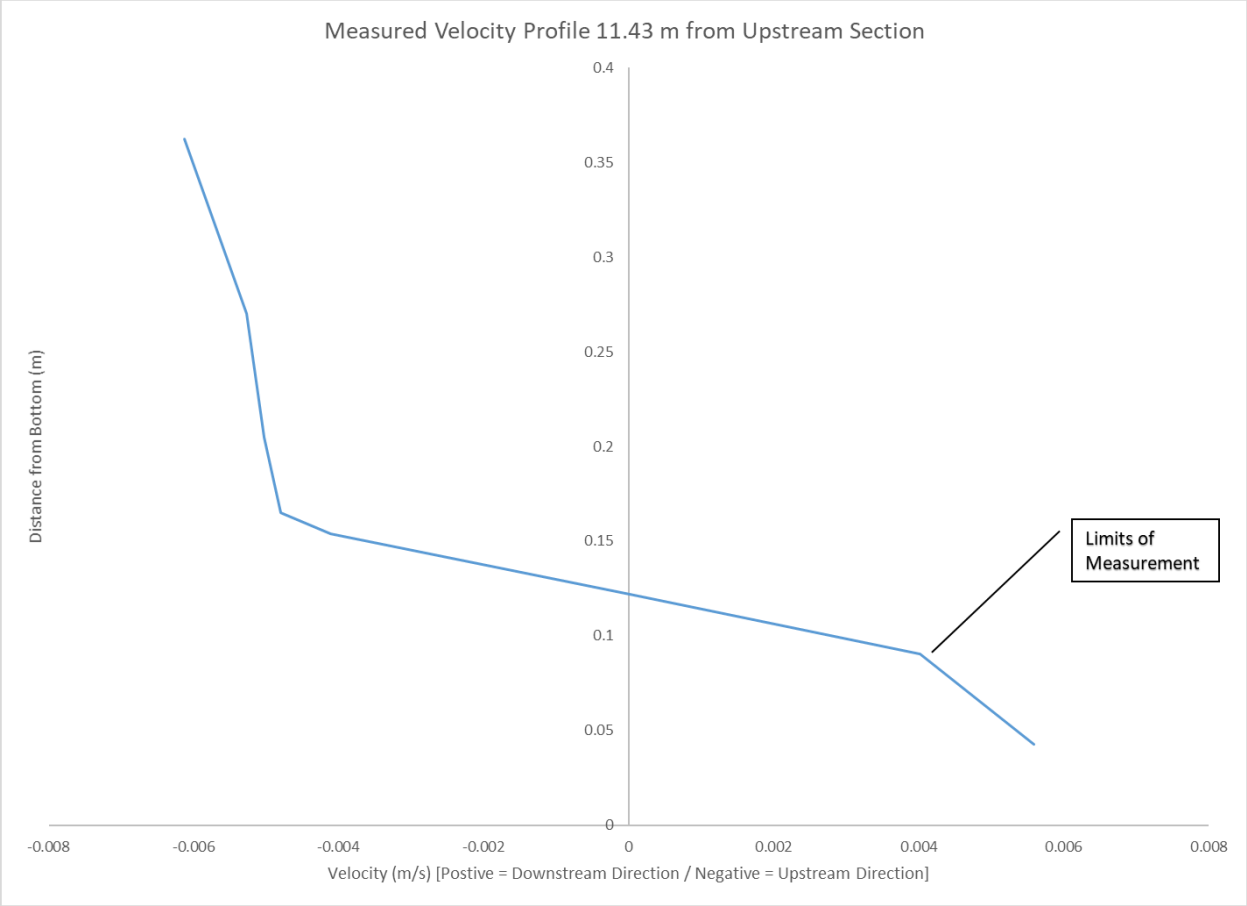

Figure 3: Recreation of measured data from Figure 14 of TR E-81-2 showing the velocity profiles of measured data and LARM run (not included here) at 11.43 meter downstream from upstream boundary. Figure 14 indicates that data was not measurable from the flume floor up to 0.10 meters above the floor.

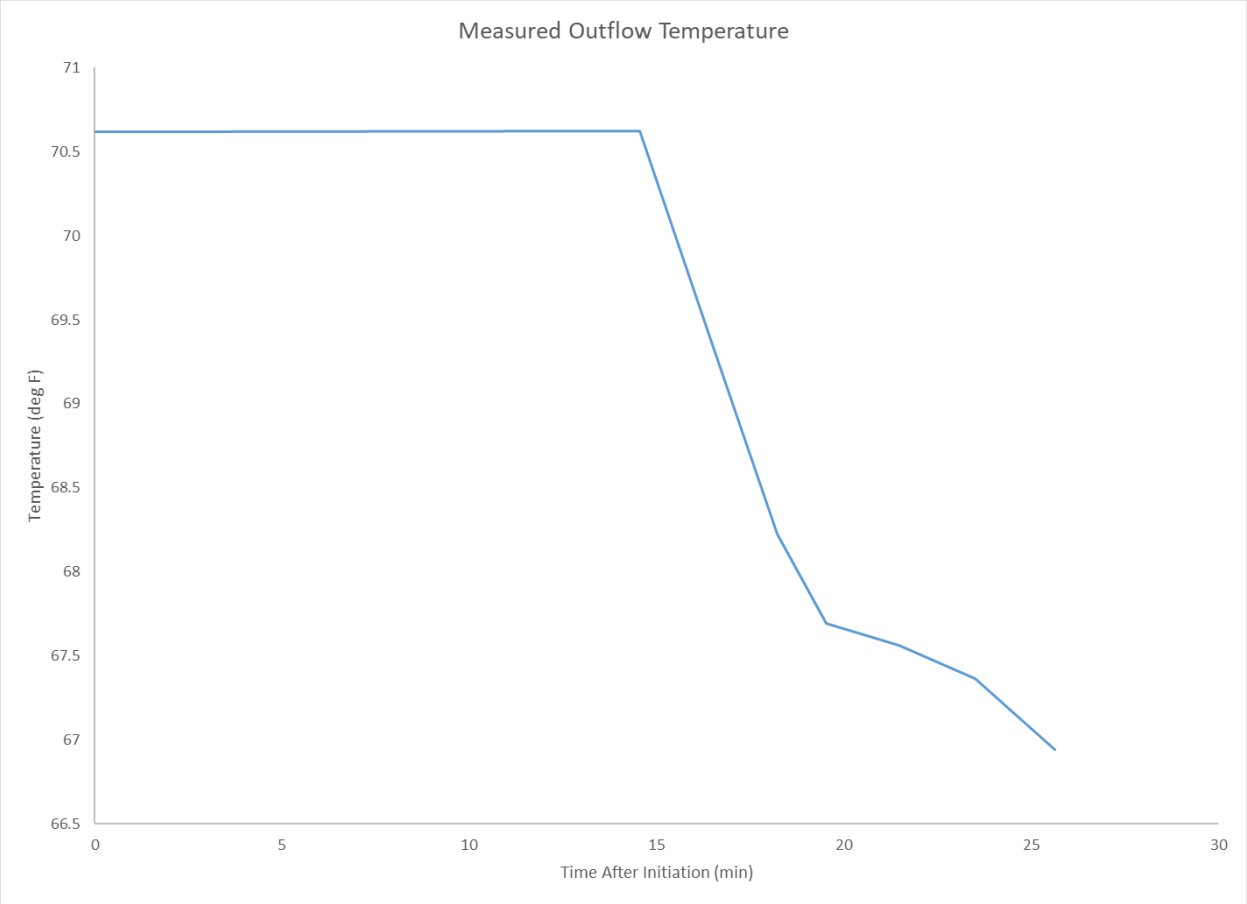

Figure 4: Recreation of measured data figure from Figure 15 of TR E-81-2 showing the recorded outflow temperature and LARM run (not included here) over approximately 26 min. Time of arrival for the underflow at the outlet is estimated between 17 and 19 minutes (Berger, et al 2014).

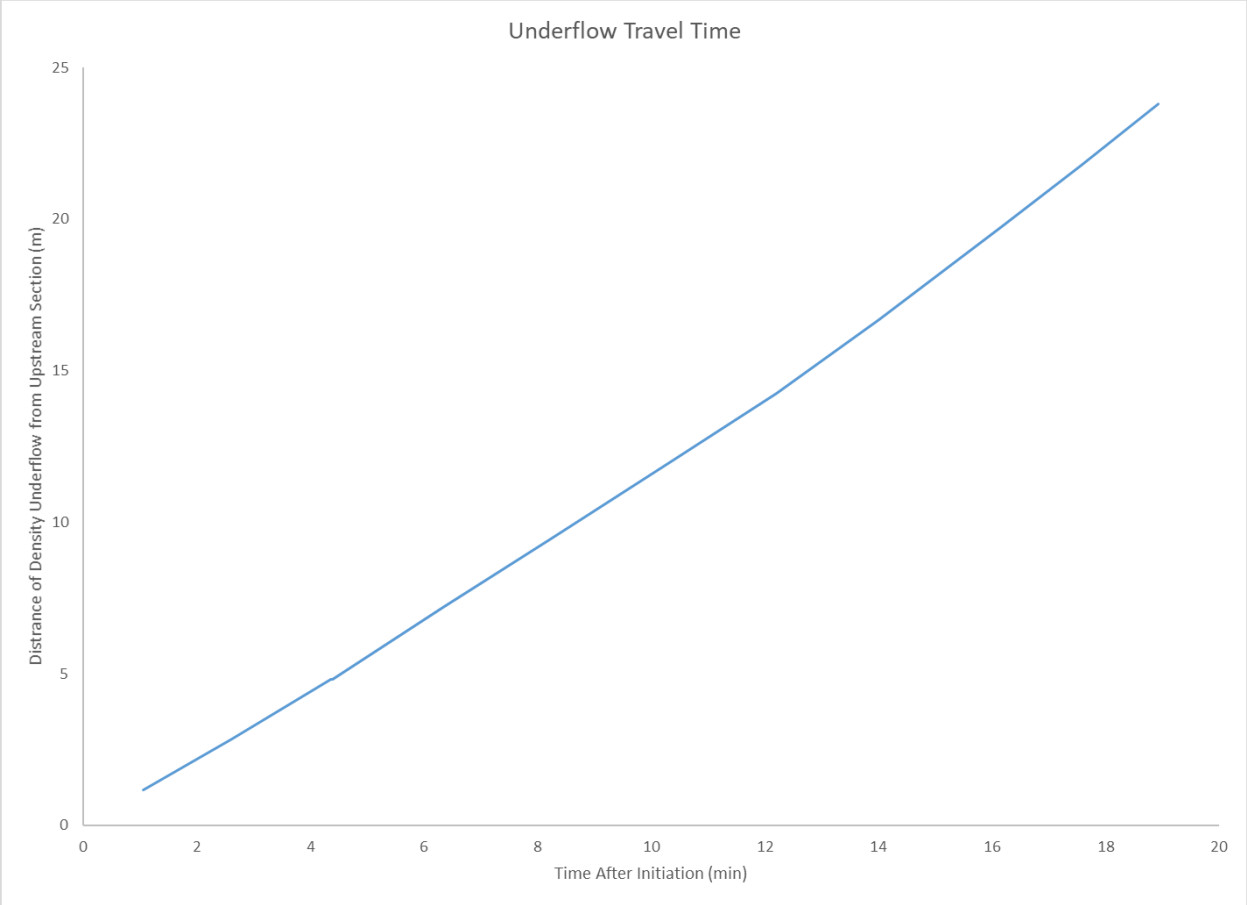

Figure 5: Recreation of measured data figure from Figure 13 of TR E-81-2 showing distance of density under flow from upstream section and time for physical model and LARM (not included here) over a period of 19 minutes.

The observational and recorded data from Johnson's study has been used in numerous subsequent validation efforts for numerical models addressing density underflow. Edinger and Buchak revisited the experimental data in Technical Report E-83-1 (Buchak and Edinger, 1983), Karpick and Raithby used the data in the development and testing of their Laterally Averaged Hydrodynamics Model (Karpick and Raithby 1990), the study data was used in Baroclinic validation tests for USACE's ADH-SW3 model assessment (Berger et al 2014) and more recently in a comparative study of vertical coordinate systems with Delft3D (Lang et al 2022).

1.2 Methods

CE-QUAL-W2 uses a z-coordinate system for the computational grid. This presents some challenges with steep floor slopes as presented in the GRH flume but may be overcome with grid

refinement. Grid resolution sensitivity and other user defined inputs are explored further in determining how to optimize a CE-QUAL-W2 model representing the GRH flume experiment.

Grid Resolution Sensitivities

Seven grids were developed to assess the effects of resolution on model accuracy. The original LARM grid dimensions from Technical Report E-81-2 were selected as the lowest resolution bathymetry file, GRH 15. An additional comparative grid resolution was selected from the Lang et al study GRH80. Subsequent grids were selected with refined resolutions to assess the effects or increasing discretization in the longitudinal and vertical coordinates, GRH 82, GRH 144, GRH326, GRH326s and GRH326d. The flume is characterized by the upstream lateral expansion (upstream) section and downstream vertically expanding (downstream) section. The grid resolutions address the upstream and downstream section slightly differently. The downstream section grid at the floor boundary can become irregular or have inconsistent longitudinal to vertical steps if the aspect ratio of the cell does not match the flume floor slope as seen in GRH 15 and GRH 80. GRH 82 and GRH 326 were developed with the same aspect ratio as the floor slope and GRH 144, GRH326s and GRH 326d were developed to assess the effected of additional longitudinal discretization without additional vertical discretization.

Table 1: Bathymetry grid resolution table show longitudinal and vertical cell dimension, cell numbers include zero value boundary conditions

Grid Name	**Upstream Section**		**Downstream Section**		**Longitudinal Cell Number**	**Vertical Cell Number**
	Δx	Δy	Δx	Δy		
GRH15	1.5240	0.0762	1.5240	0.0762	17	14
GRH80	0.3050	0.0252	0.3050	0.0252	81	38
GRH82	0.3050	0.0100	0.2998	0.0100	83	92
	--	--	0.2998	0.0101		
GRH 144	0.3050	0.0100	0.1499	0.0100	144	92
	--	--	0.1499	0.0101		
GRH326	0.0762	0.0100	0.0749	0.0100	326	92
	--	--	0.0749	0.0101		
GRH326s	0.0762	0.0200	0.0749	0.0200	326	47
	--	--	0.0749	0.0203		
GRH326d	0.0762	0.0500	0.0749	0.0050	326	182
	--	--	0.0749	0.0050		

Input Parameter Sensitivities

Additional input parameter sensitivities were conducted on GRH326 model bathymetry to further assess potential for optimization.

Sensitivities to Manning's n

Sensitivity to the roughness coefficient was conducted with GRH326. Manning's n for smooth glass, n = 0.009 (Sturm 2001), was used as a default value. CE-QUAL-W2 limits manning roughness values to 0.00001, which although unrealistic, was used as a limit determining sensitivity to reduction.

Inflow placement

Placement of inflow based on relative density for the full upstream boundary is the default application for this exercise. Distributed placement was evaluated for GRH326 as well as mid-water column elevation and top of water column elevation with relative density placement. These upper elevation relative inflow density placements were accomplished by making perching the upstream boundary on a single cell width shelf.

Longitudinal Eddy Viscosity

Longitudinal eddy viscosity controls the horizontal dispersion of momentum. This input was evaluated at 1.50E-6 m^2/s and 1.00E-9 m^2/s. 1.50E-6 m^2/s was the value estimated and applied within TR-E-81-2 (Johnson 1981). 1.00E-9 m^2/s was used for verification and validation of ADH-SW3 in ERDC-TR-14-7 (Berger 2014).

Maximum Eddy Viscosity

Vertical eddy viscosity controls the vertical dispersion of momentum. CE-QUAL-W2 calculates the vertical eddy viscosity using a Turbulent Kinetic Energy, kε turbulent closure, model internally. The maximum vertical eddy viscosity can be restricted and for the purpose of evaluating the influence, it was varied from 1.50E-6 m^2/s to 1.00E-9 m^2/s.

Geometry and Starting Water Surface

Due to an inconsistency in flume width documentation for the GRH flume, an additional bathymetry file of GRH326 with maximum channel width of 2.85 ft as described in TR-E-85-14

(Dortch et al 1985) was developed and run. The GRH flume schematic from TR-E-85-14 is include below in Figure 6.

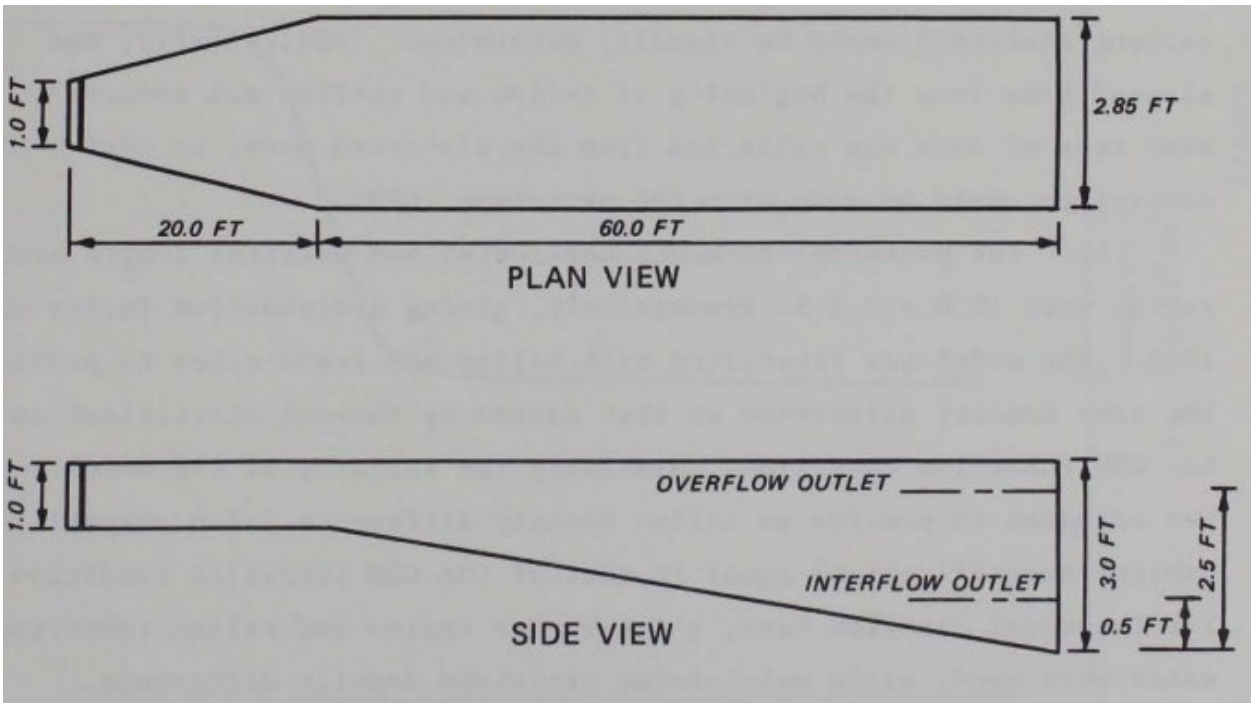

Figure 6: Schematic of GRH flume from TR-E-85-14 (Figure 6) indicating a narrower flume width than reported in TR-E-81-2.

Additionally, the starting water surface was set at 2 centimeters above and 4 centimeters below the reported elevation of 0.91 meter in TR-E-81-2 and GRH326 was rerun. The water surface sensitivity was conducted due to lack of explicit water surface elevation documentation along the flume and indications of a water surface elevation 0.42 meters at the velocity profile. Though it is unclear if the water surface indicated is modeled or observed. Assuming a zero hydraulic slope, the depth of water at the horizontal velocity transect should be 0.48 meters.

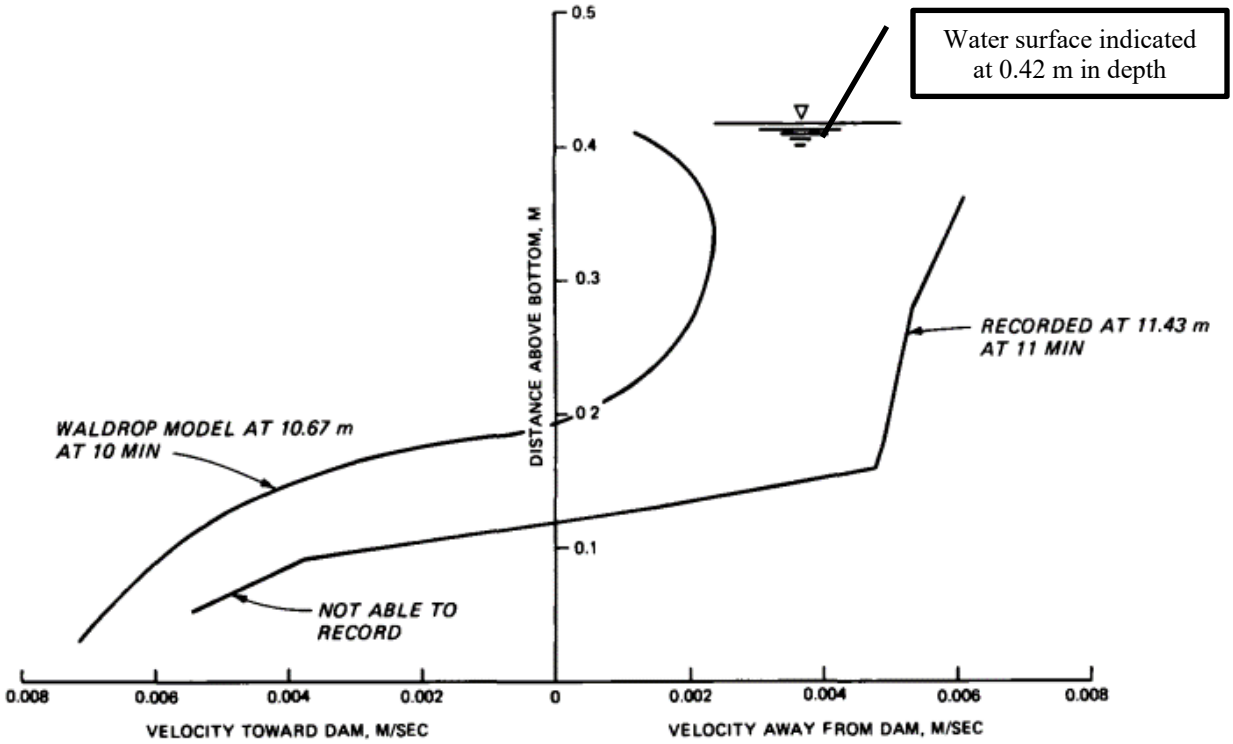

Figure 7: Horizontal velocity profile at 11.43 meters indicating a water surface (Figure 41, Johnson 1981). This figure was digitized to determine the depth indicated.

Assessment Metrics

Two metrics were selected for assessing the performance of each model iteration, time of arrival and depth at velocity direction change. Time of arrival refers to the estimated time at which the density underflow begins to exit the outflow port. This has been used as an assessment metric in several of the other numerical studies benchmarking against the GRH flume results. Berger et al report time of arrival as 17 to 19 minutes with a benchmark time of 18 mins in ERDC-TR-14-7. This time of 18 minutes was adopted for the time of arrival metric target. Additionally, other studies used the velocity profile as a direct comparison between the physical model and numerical models; however, for this effort a single depth at velocity direction change was selected as a quantitative assessment for CE-QUAL-W2 model iteration. The depth at velocity direction change is indicative of the depth of velocity underflow. The reported velocity profile from physical model has limited depth range as a result of the collection method and only recorded velocity from about 0.05 meters to 0.37 meters.

1.3 Results

Grid Resolution Sensitivities

The effect of the grid resolution on the performance metrics is present in Table 2. Most model runs rendered acute temperature drop in the outflow temperature time series indicating the time of arrival. GRH15 did not yield a distinctive temperature drop and did not result in bidirectional flow at the transect show in Figure 8.

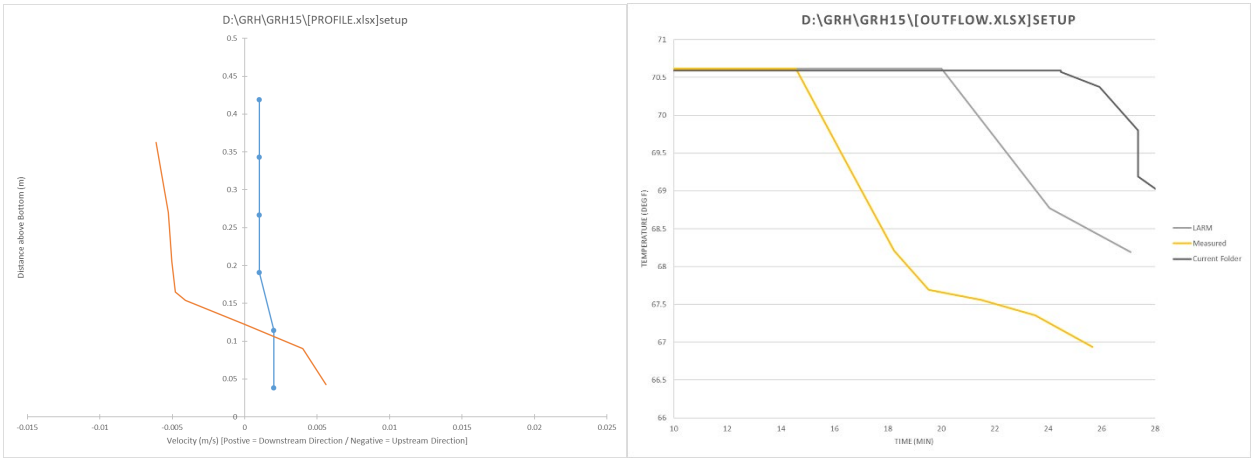

Figure 8: Velocity profile (left) and temperature-time series of outflow (right) for GRH15.

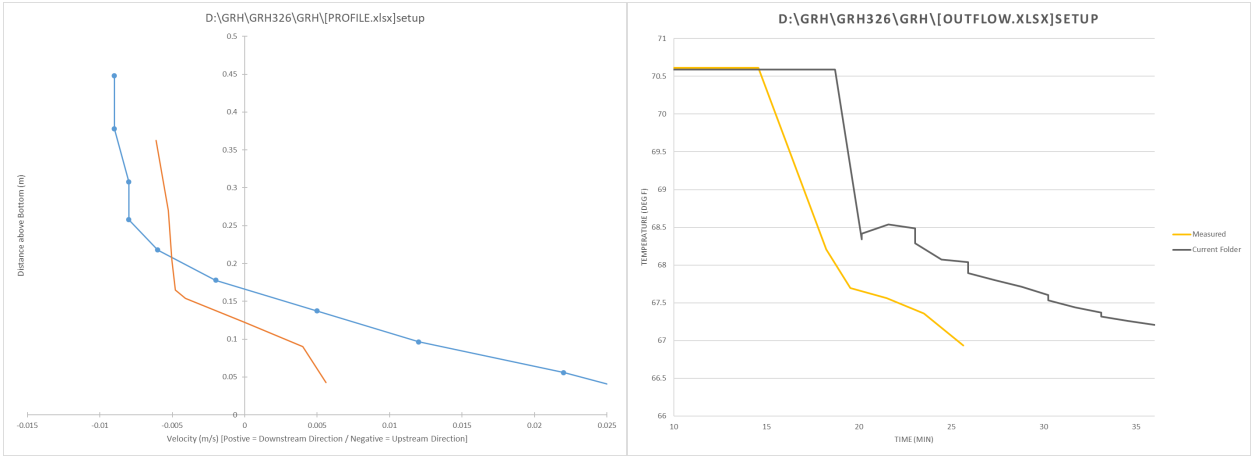

Figure 9: Velocity profile (left) and temperature-time series of outflow (right) for GR326.

Table 2: Grid Resolution performance table. GRH 15 did not present a distinctive time of arrival and did not render bidirectional flow at the velocity transect.

Model	Cell Count	Time of Arrival	Error	Depth at Velocity	Error

	(Length X Depth)	(min)		Direction Change (m)	
GRH15	17 X 14	28.0	56%	NA	
GRH80	81 X 92	24.5	36%	0.18	44%
GRH82	83 X 92	21.6	20%	0.2	60%
GRH144	144 X 92	20.2	12%	0.17	36%
GRH 326	326 X 92	20.1	12%	0.165	32%
GRH326d	326 X 47	20.1	12%	0.19	52%
GRH326s	326 X 182	20.1	12%	0.145	16%
Physical		18		0.125	

Subsequent model iterations of increased grid resolution presented improvements in time of arrival. However, this improvement by increased grid resolution appears limited. Grid resolution had a more varied effect on accuracy of the predicted change in velocity direction depth. A decreased longitudinal cell dimension demonstrated improvements to the underflow thickness as noted from GRH82 to GRH144. Subsequently, cell thickness has the opposite effect as noted in GRH326, GRGH326s, and GRH326d. Thicker cells of GRH326s appear to reduce error in the density underflow thickness. It is noted that thinner cells with density placed inflow increases the localized inflow velocity which in turn increases mixing and result in entrainment of the at-rest warm water. This is evident at the upstream boundary in Figure 9, This effect is addressed in greater detail in Conclusions.

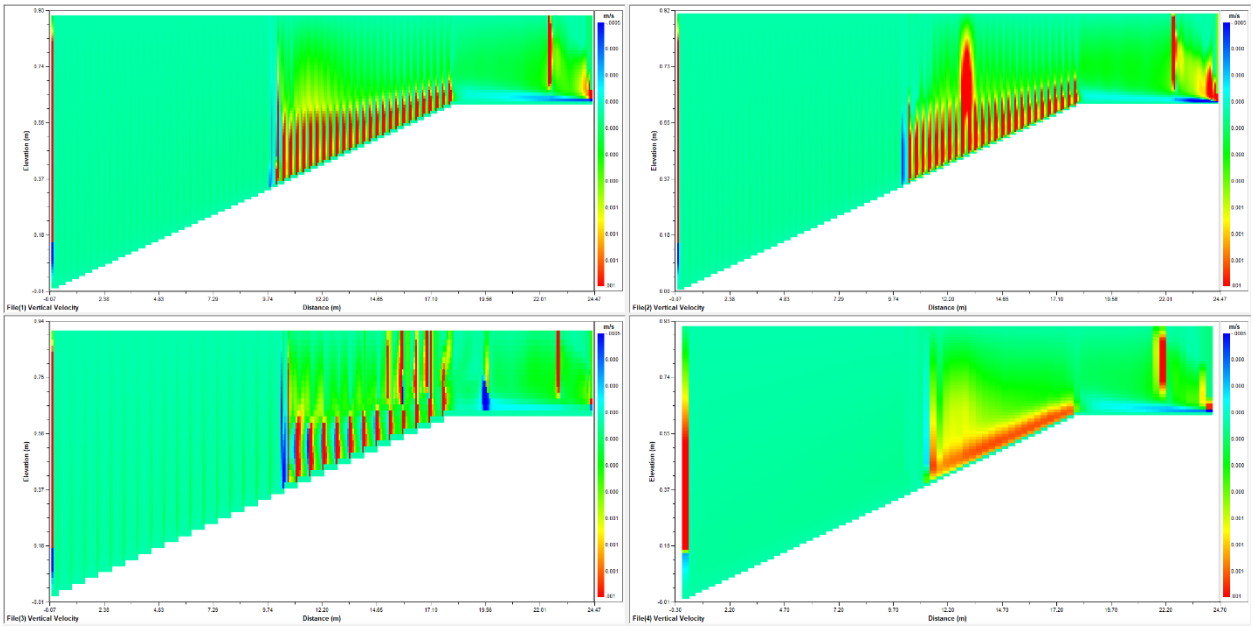

Figure 10: Vertical velocity color plot of GRH326 (upper left), GRH326d (upper right), GRH326s (lower left), and GRH82 (lower right).

Input Parameter Sensitivities

Input parameter changes for GRH326 presented additional reduction in error in time of arrival and depth at velocity change. Table 3 presents the results of 4 input parameter modifications. Eddy Viscosity Change 1 represents a model run with the longitudinal eddy viscosity set at 1.00E-9 m^2/s and maximum vertical eddy viscosity set to 1.00E-6 m^2/s. Eddy Viscosity Change 2 represents a model run with the longitudinal eddy viscosity set at 1.00E-9 m^2/s and maximum vertical eddy viscosity set to 1.00E-9 m^2/s. Negligible improvements we noted in changing the longitudinal eddy viscosity; however, significant error reduction in the time of arrival occurred with the reduction to the vertical eddy viscosity limit. Vertical eddy viscosity also has a small impact in reducing the error in the depth at velocity change. Manning's n was changed from the default value of 0.009 to 0.007 presented in the modification reported below. Significant improvements occurred in time of arrival but not impact to depth at velocity change. Additional runs not reported in this table with lower Manning's n values did not yield any additional significant improvements in time of arrival indicating a limit of influence. Distributed inflow resulted in delayed time of arrival and the elevated depth at velocity direction change.

Table 3: Effect of input parameter sensitivities table.

Model	Modification	Time of Arrival (min)	Error	Depth at Velocity Direction Change (m)	Error
GRH326	No Mod	20.1	12%	0.165	32%
	Eddy Viscosity Change 1	20.1	12%	0.165	32%
	Eddy Viscosity Change 2	18.7	4%	0.16	28%
	Manning's n = 0.007	18.7	4%	0.165	32%
	Distributed Flow	21.6	20%	0.18	44%
Physical		18		0.125	

Results of the additional inflow placements were not included in the summary table above. The perched placements with density placed inflow resulted in high velocity jets interacting with the submerged weir baffle. In several cases, underflow did not register or develop at the velocity profile station below. At temperature color plot is shown below in Figure 9.

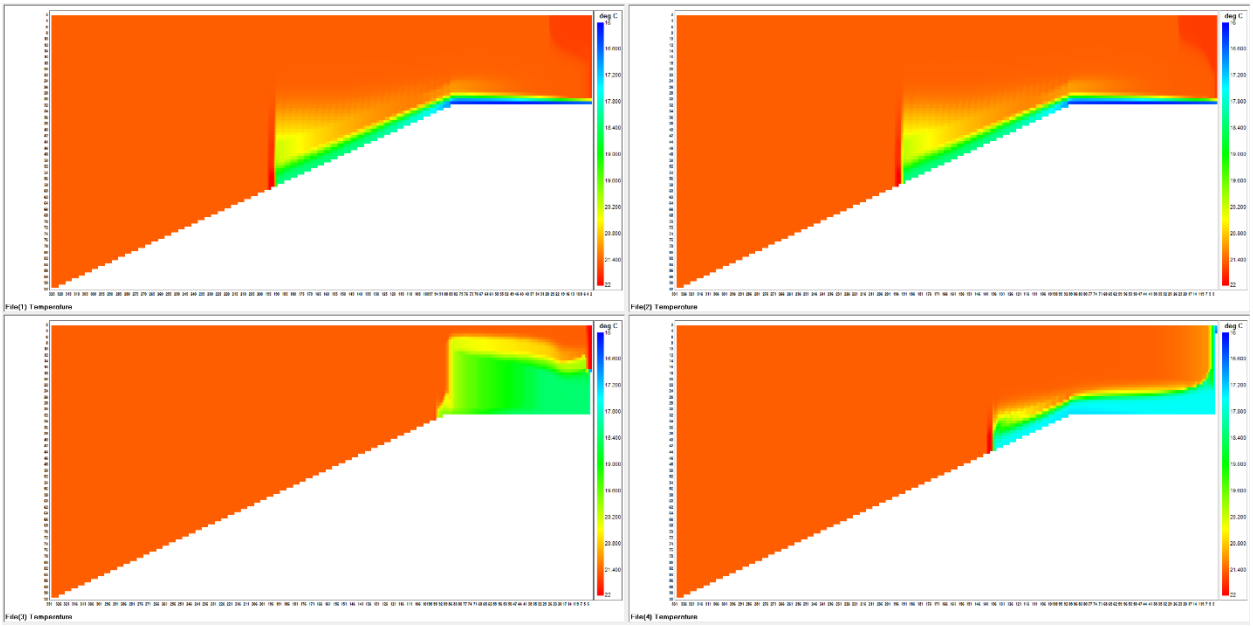

Figure 11: Temperature contour plots of GRH326 (upper left), GRH326 bottom placement (upper right), GRH326 mid depth placement (lower left) and GRH326 upper placement (lower right).

Additional detail for model results may be found in the Appendices with velocity profile and temperatures time series for outflow of models discussed here.

2.0 CONCLUSIONS

The results of the grid resolution assessment demonstrate the importance of selecting appropriate scale to the model development. Due to the application of the density inflow placement in CE-QUAL-W2 vertical grid scale at the upstream boundary has a pronounced effect. With the density difference of the initial condition flume water and in the incoming cold water, the density placement inflow is confined to the deepest layer of the boundary. Increasing the vertical resolution at the boundary results in greater inflow velocities. These higher velocities result in greater mixing and thereby a thicker underflow depth at the velocity profile station. Using the density placement inflow function requires selection of an appropriate cell thickness that represents the inflow near the boundary. On the other hand, distributed inflow at the boundary was not suitable in this application and greatly misrepresented inflow conditions. Further assessment should focus on optimizing the vertical scale for the top 0.3 meters of the flume to represent the underflow velocity at or near the boundary. Alternatively, a code modification to force distributed flow through a lower region or cell range of the boundary may support this assessment. The lower 0.61 meters of the grid representing the sloped floor may benefit from the increased vertical resolution after the underflow has fully developed. Increasing longitudinal grid resolution appears to have some limited benefits.

Adjusting other input parameters, specifically friction and vertical eddy viscosity limits, provide additional means of optimization. Combining these parameter adjustments with an optimized grid may yield improved replication of the physical study.

Given the limited description of the GRH flume study supporting TR-E-81-2, additional research into the implementation of the physical study may help better define the numerical model inputs. Various inconsistencies noted in research of the GRH flume were tested within this assessment CE-QUAL-W2 and were found to have minor effect. Supporting documentation or interviews with ERDC CHL personnel may provide additional detail such as water surface limitation of the flume and flume width.

3.0 REFERENCES

1. Berger, R. C., McAlpin, T., Savant, G., Trahan, C., Three-Dimensional Shallow-Water Adaptive Hydraulics (ADH-SW3): Hydrodynamic Verification and Validation. Technical Report 14-7. Vicksburg, MS: ERDC Coastal and Hydraulics Laboratory.

2. Dortch, M., Holland, J., Wilhelms, S. 1985. Physical Modeling of Reservoir Hydrodynamics. Technical Report E-85-14. Vicksburg, MS: U.S. Army Engineer Waterways Experiment Station.

3. Edinger, J., Buchak, E. 1983. Developments in LARM2: A longitudinal-vertical, time-varying hydrodynamic reservoir model. Technical Report E-83-1. Vicksburg, MS: U.S. Army Engineer Waterways Experiment Station.

4. Johnson, B. H. 1981. A review of numerical reservoir hydrodynamic modeling. Technical Report E-81-2. Vicksburg, MS: U.S. Army Engineer Waterways Experiment Station.

5. Karpik, S. R., Raithby, G. D. Laterally averaged hydrodynamics model for reservoir predictions. United States: N. p., 1990. Web. doi:10.1061/(ASCE)0733-9429(1990)116:6(783).

6. Lang, Y.; Hu, Z.; Hao, R.; Li, Y.; Han, L. Comparative Study on Water Temperature Stratified Flow under Different Vertical Coordinate Systems in Delft3D. Water 2022, 14, 2737. https://doi.org/10.3390/ w14172737

7. Sturm, T. W. (2001). *Open channel hydraulics*. McGraw-Hill.

8. Wells, S. A., editor (2023) "CE-QUAL-W2: A two-dimensional, laterally averaged, hydrodynamic and water quality model, version 4.5, user manual part 1, introduction," Department of Civil and Environmental Engineering, Portland State University, Portland, OR.

4.0 APPENDICES

Model Data Presented June 6, 2023

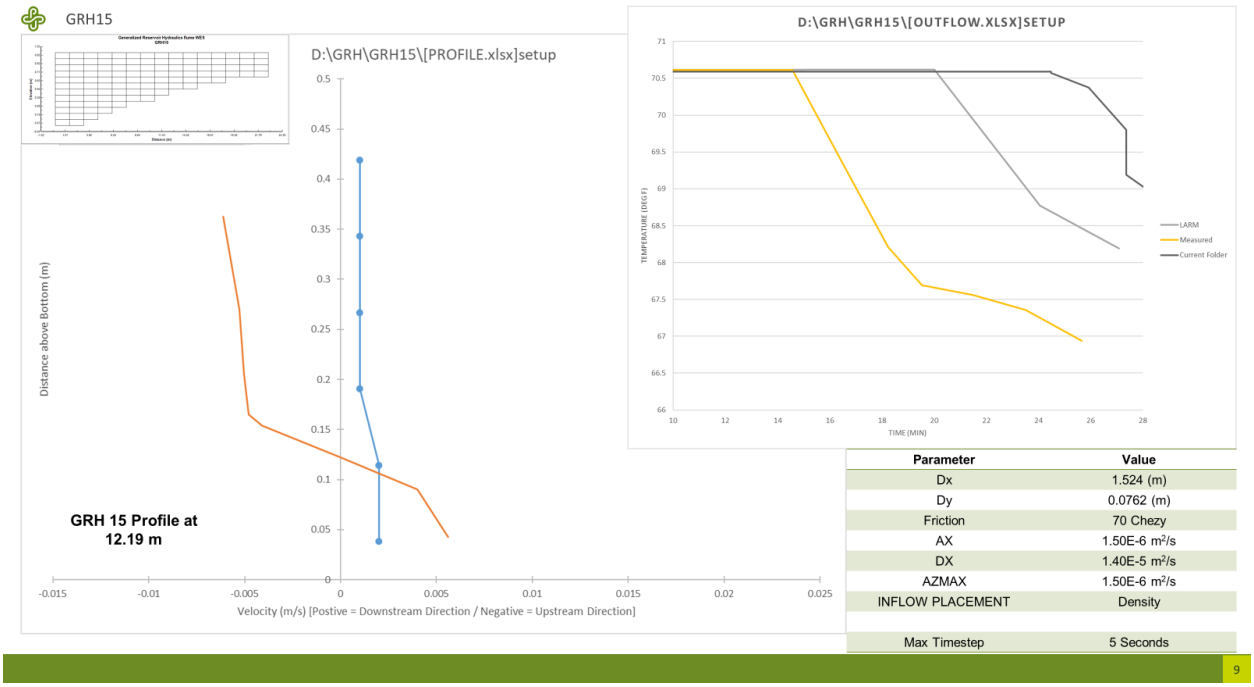

Parameter	Value
Dx	1.524 (m)
Dy	0.0762 (m)
Friction	70 Chezy
AX	1.50E-6 m^2/s
DX	1.40E-5 m^2/s
AZMAX	1.50E-6 m^2/s
INFLOW PLACEMENT	Density
Max Timestep	5 Seconds

9

Figure 12: GRH15 model results.

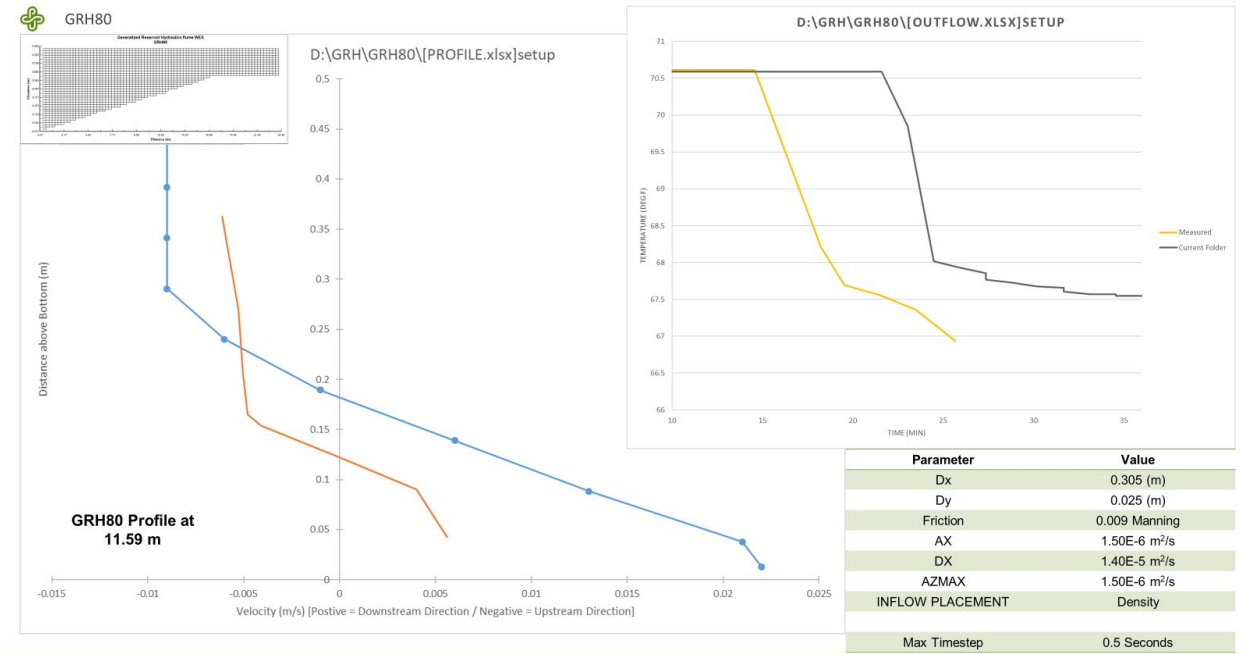

Parameter	Value
Dx	0.305 (m)
Dy	0.025 (m)
Friction	0.009 Manning
AX	1.50E-6 m^2/s
DX	1.40E-5 m^2/s
AZMAX	1.50E-6 m^2/s
INFLOW PLACEMENT	Density
Max Timestep	0.5 Seconds

10

Figure 13: GRH80 model results.

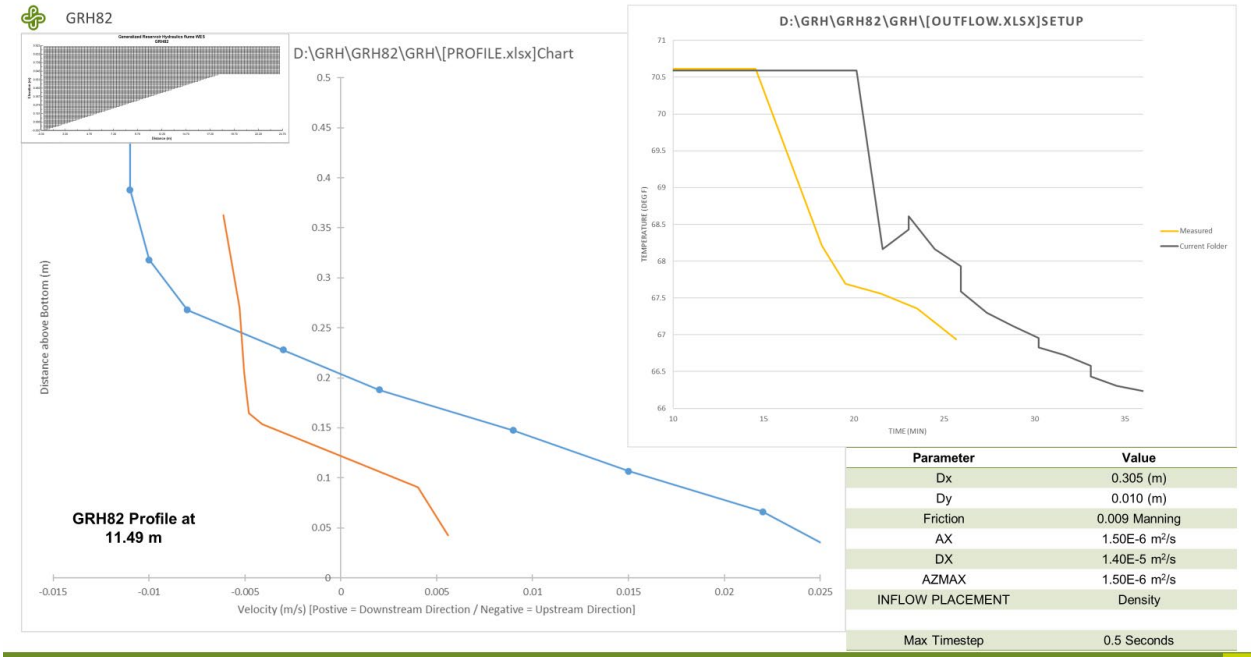

Figure 14: GRH 82 model results.

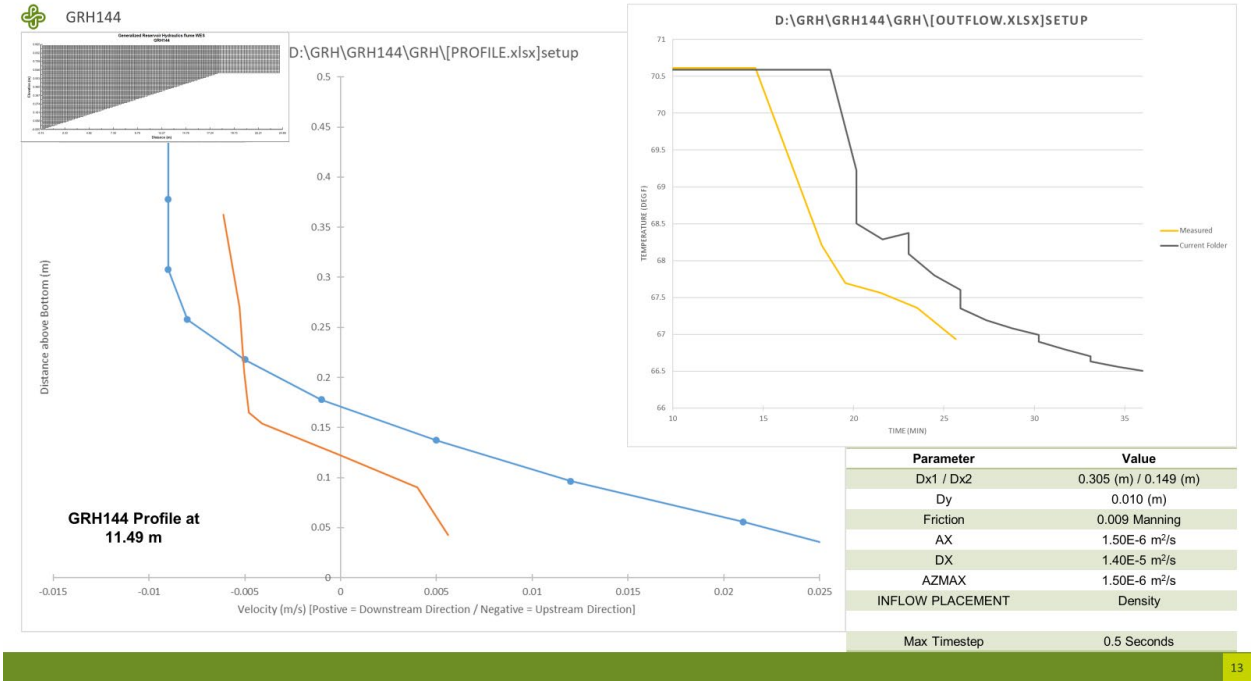

Figure 15: GRH 144 model results.

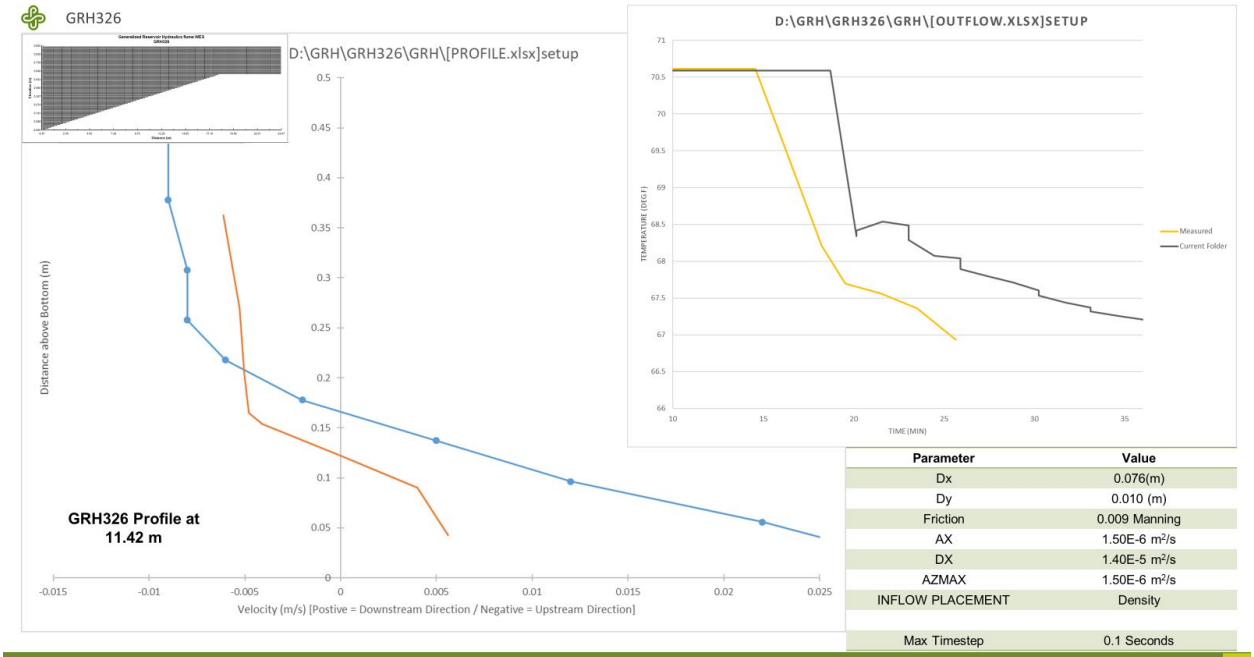

Parameter	Value
Dx	0.076(m)
Dy	0.010 (m)
Friction	0.009 Manning
AX	1.50E-6 m^2/s
DX	1.40E-5 m^2/s
AZMAX	1.50E-6 m^2/s
INFLOW PLACEMENT	Density
Max Timestep	0.1 Seconds

14

Figure 16: GRH326 model results.

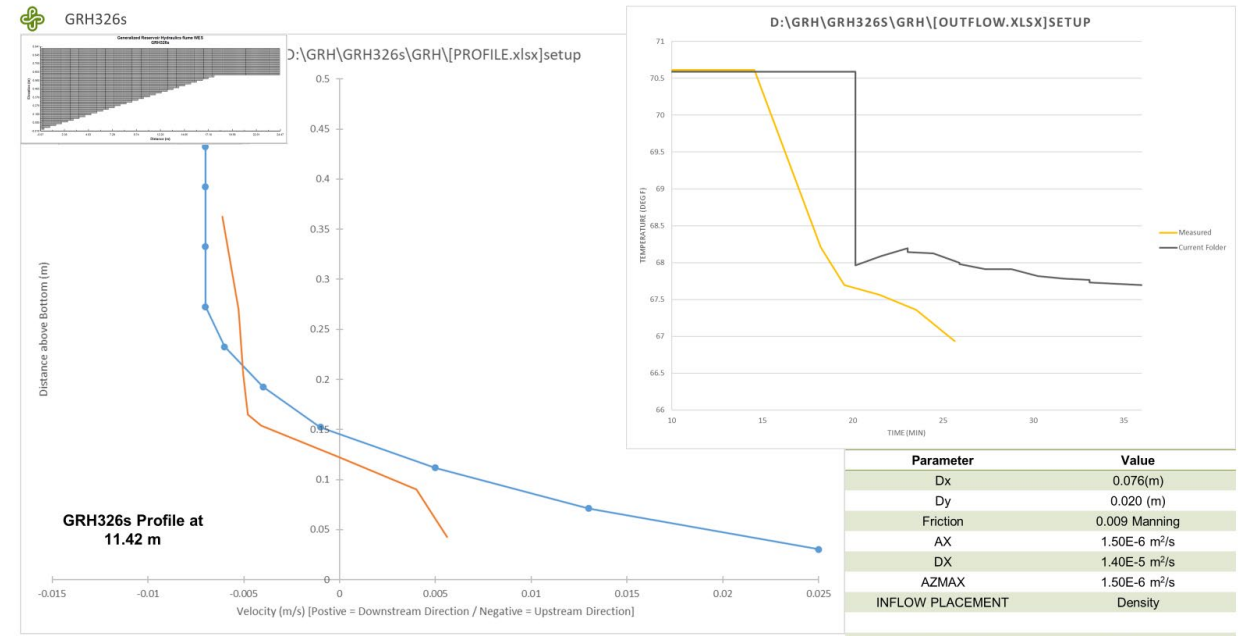

Parameter	Value
Dx	0.076(m)
Dy	0.020 (m)
Friction	0.009 Manning
AX	1.50E-6 m^2/s
DX	1.40E-5 m^2/s
AZMAX	1.50E-6 m^2/s
INFLOW PLACEMENT	Density
Max Timestep	0.1 Seconds

15

Figure 17: GRH326s model results.

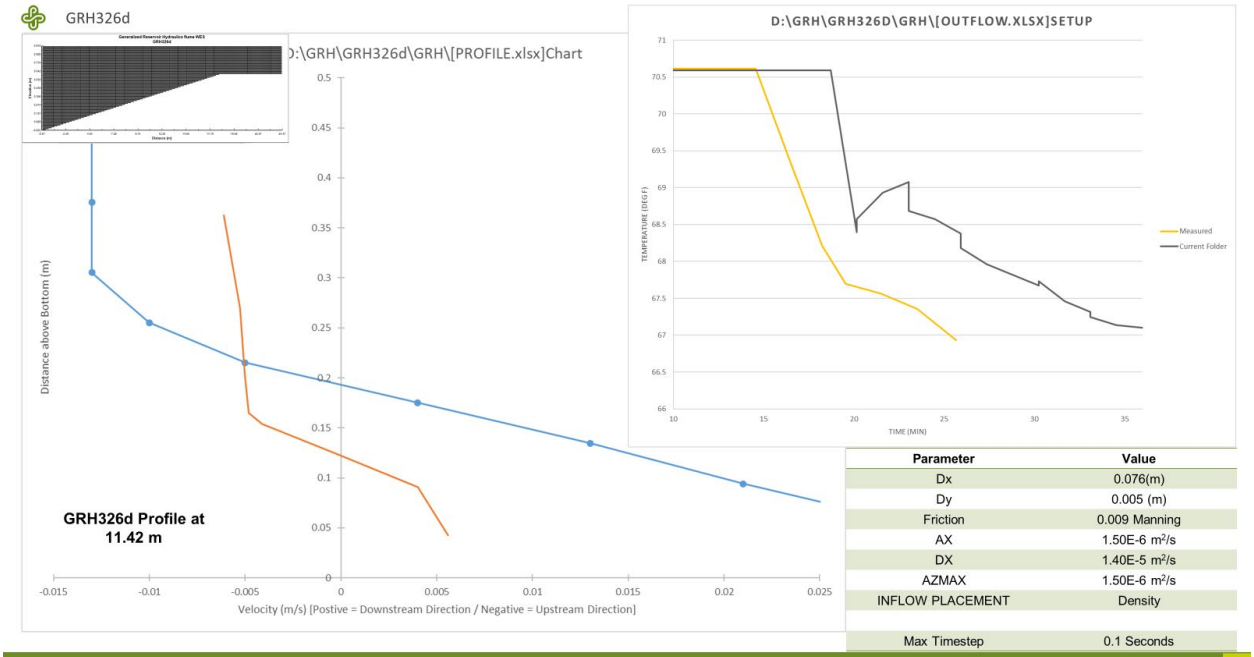

Parameter	Value
Dx	0.076(m)
Dy	0.005 (m)
Friction	0.009 Manning
AX	1.50E-6 m^2/s
DX	1.40E-5 m^2/s
AZMAX	1.50E-6 m^2/s
INFLOW PLACEMENT	Density
Max Timestep	0.1 Seconds

16

Figure 18: GRH 326d model results.

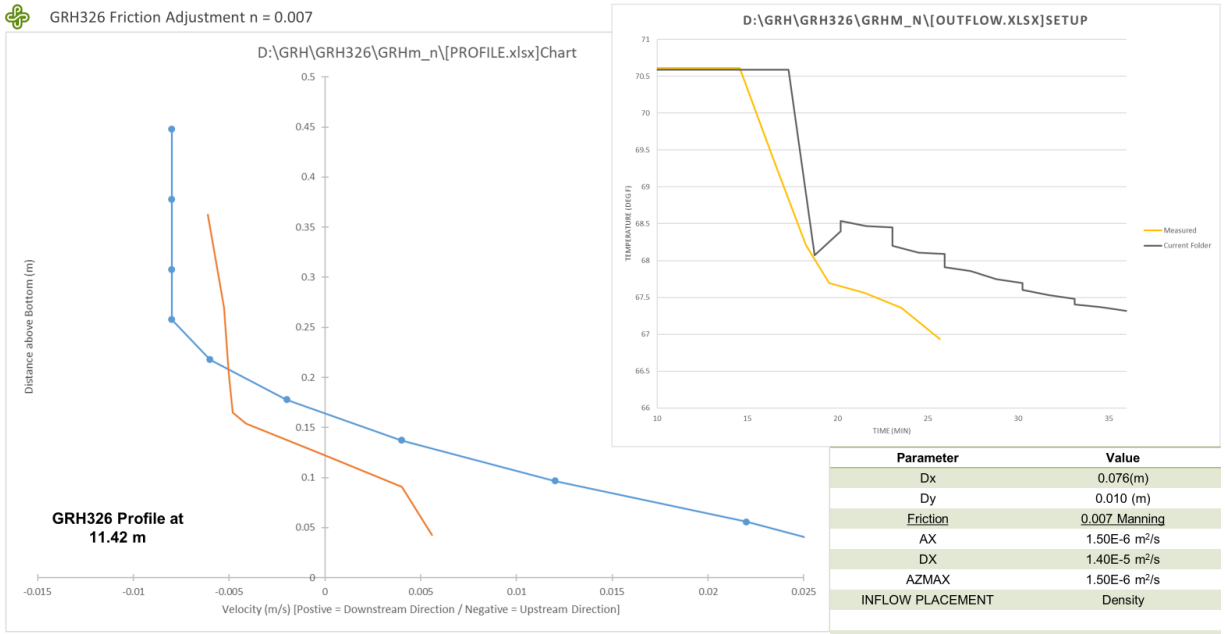

Parameter	Value
Dx	0.076(m)
Dy	0.010 (m)
Friction	0.007 Manning
AX	1.50E-6 m^2/s
DX	1.40E-5 m^2/s
AZMAX	1.50E-6 m^2/s
INFLOW PLACEMENT	Density
Max Timestep	0.1 Seconds

22

Figure 19: GRH 326 Manning n = 0.007 model results.

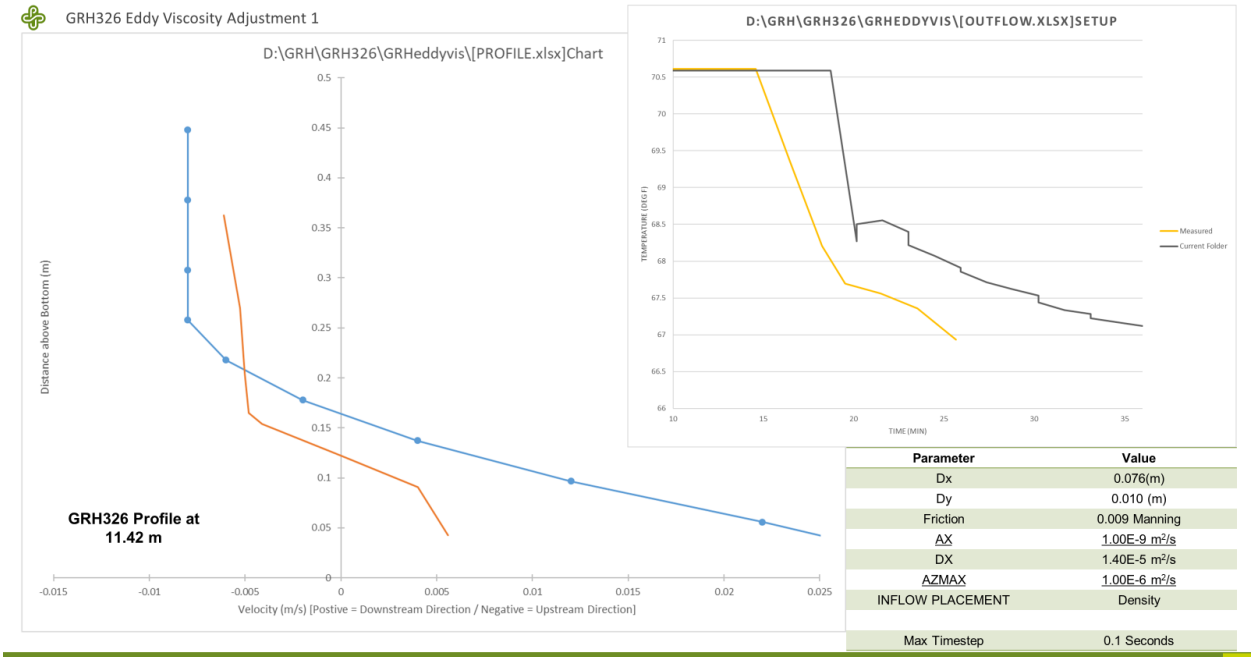

Figure 20: GRH326 Eddy Vis. 1 model results.

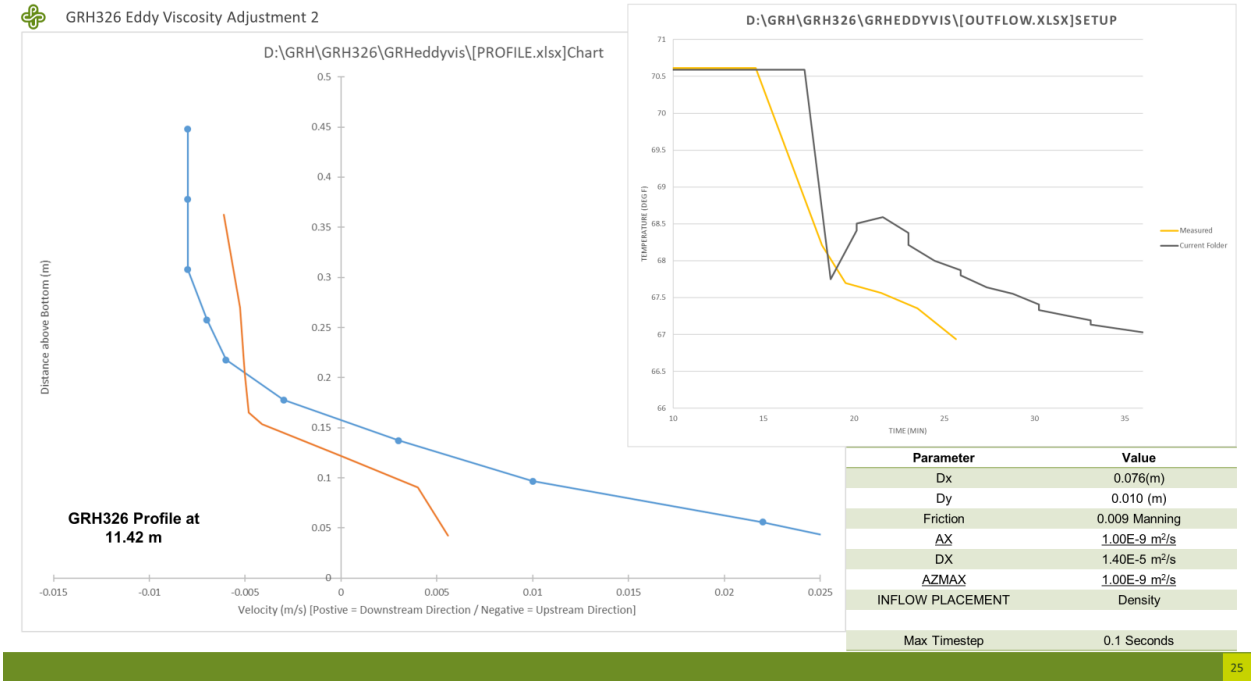

Figure 21: GRH 326 Eddy Vis. 2 model results.

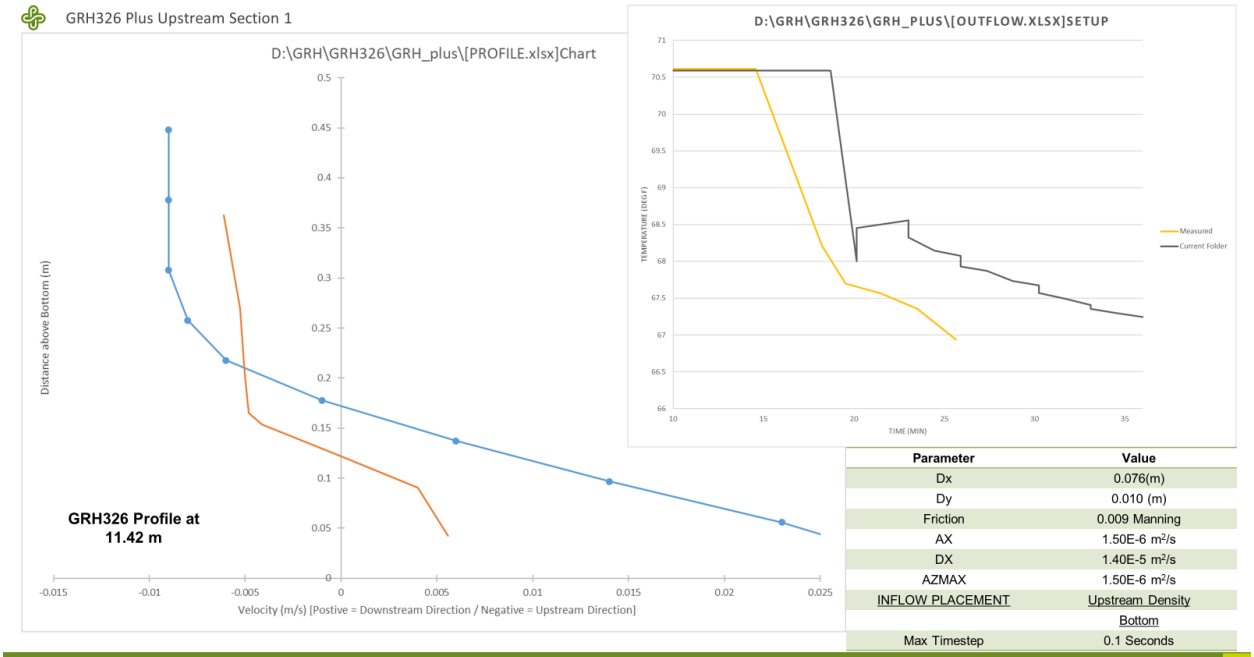

Parameter	Value
Dx	0.076(m)
Dy	0.010 (m)
Friction	0.009 Manning
AX	1.50E-6 m^2/s
DX	1.40E-5 m^2/s
AZMAX	1.50E-6 m^2/s
INFLOW PLACEMENT	Upstream Density Bottom
Max Timestep	0.1 Seconds

27

Figure 22: GRH326 bottom placement model results.

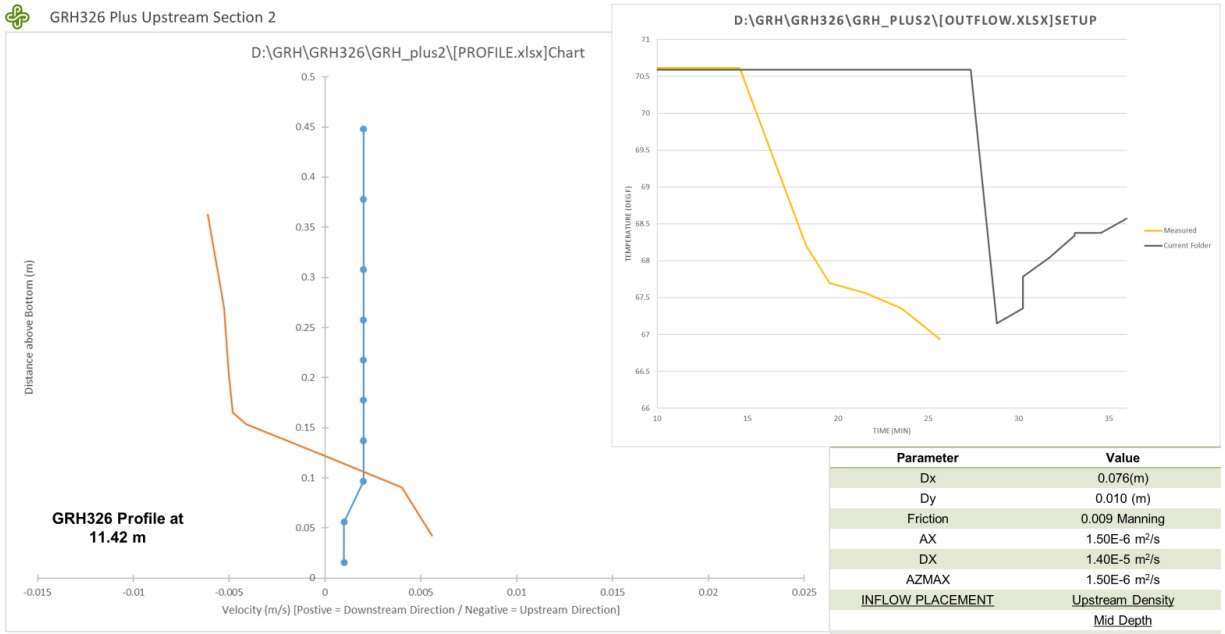

Parameter	Value
Dx	0.076(m)
Dy	0.010 (m)
Friction	0.009 Manning
AX	1.50E-6 m^2/s
DX	1.40E-5 m^2/s
AZMAX	1.50E-6 m^2/s
INFLOW PLACEMENT	Upstream Density Mid Depth
Max Timestep	0.1 Seconds

28

Figure 23: GRH 326 mid depth placement model results.

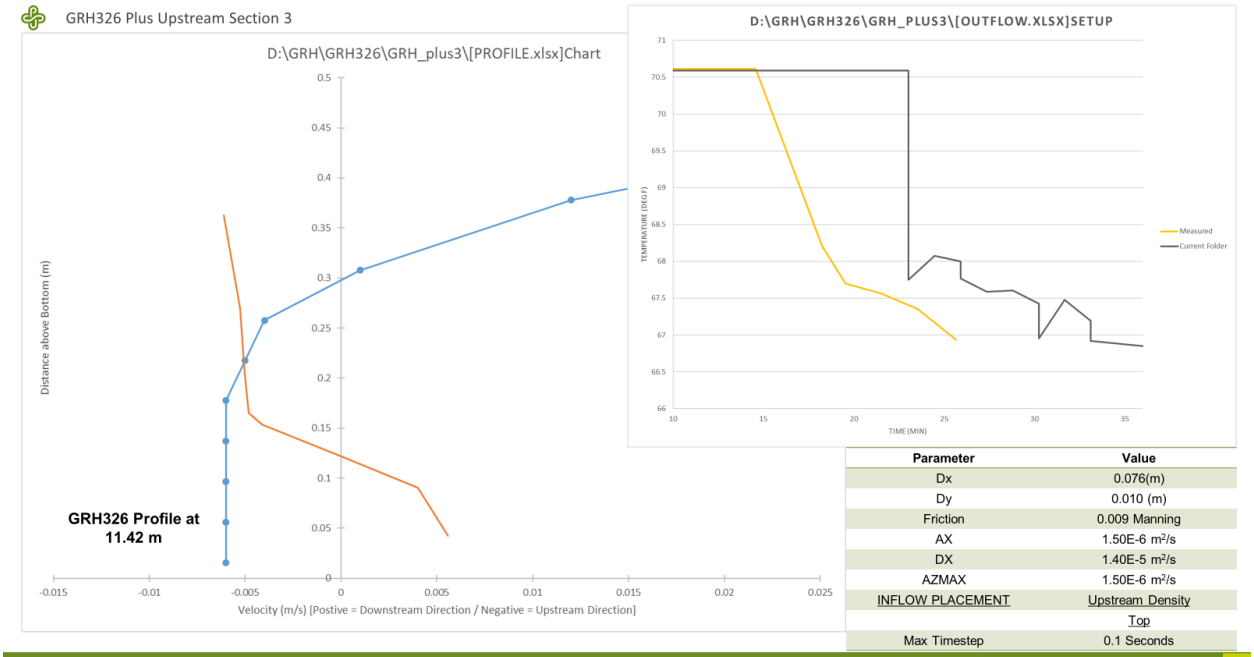

Parameter	Value
Dx	0.076(m)
Dy	0.010 (m)
Friction	0.009 Manning
AX	1.50E-6 m^2/s
DX	1.40E-5 m^2/s
AZMAX	1.50E-6 m^2/s
INFLOW PLACEMENT	Upstream Density
	Top
Max Timestep	0.1 Seconds

29

Figure 24: GRH 326 top placement model results.

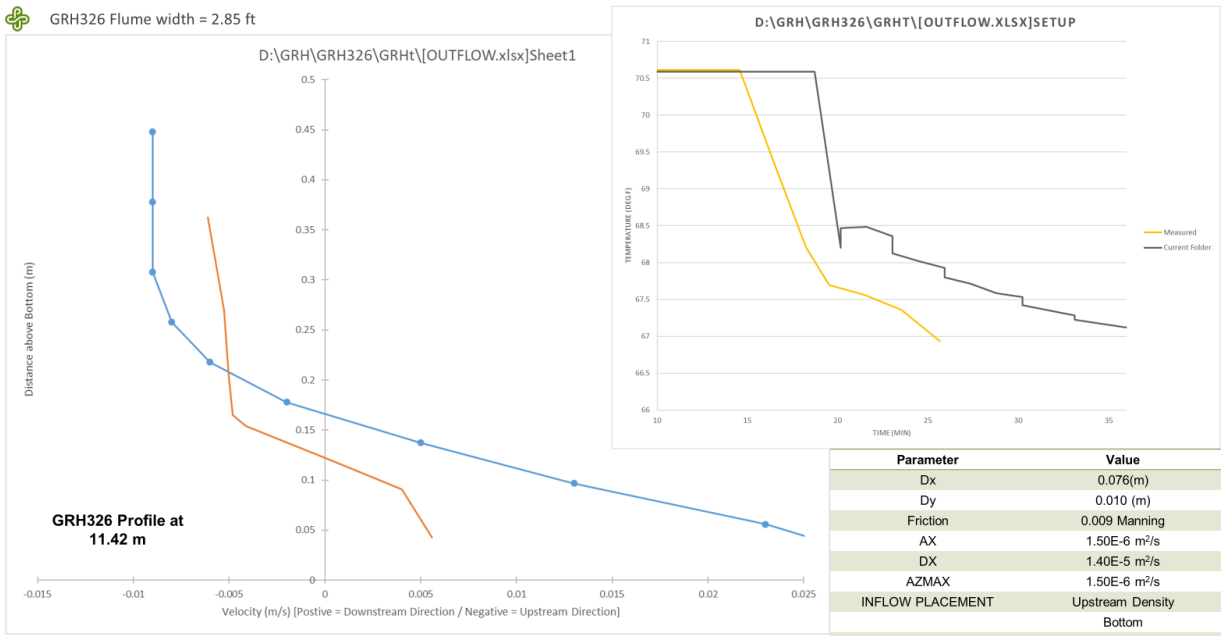

Parameter	Value
Dx	0.076(m)
Dy	0.010 (m)
Friction	0.009 Manning
AX	1.50E-6 m^2/s
DX	1.40E-5 m^2/s
AZMAX	1.50E-6 m^2/s
INFLOW PLACEMENT	Upstream Density
	Bottom
Max Timestep	0.1 Seconds

33

Figure 25: GRH 326 narrow flume model results.

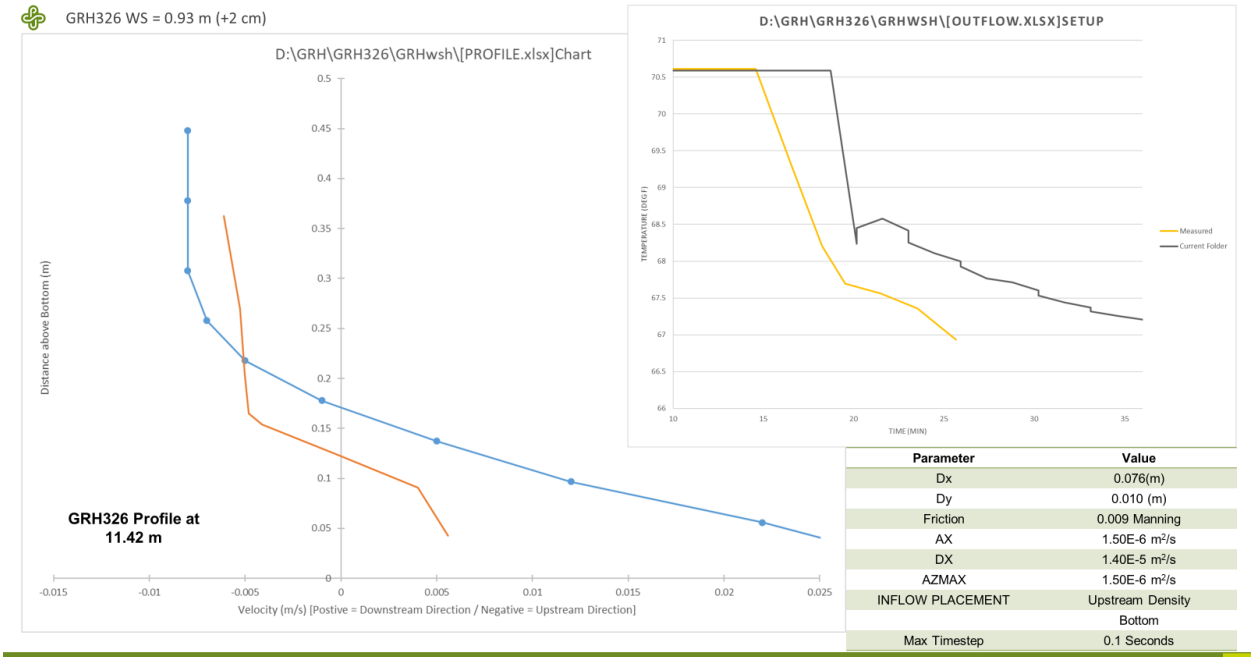

Figure 26: GRH326 high water surface model results.

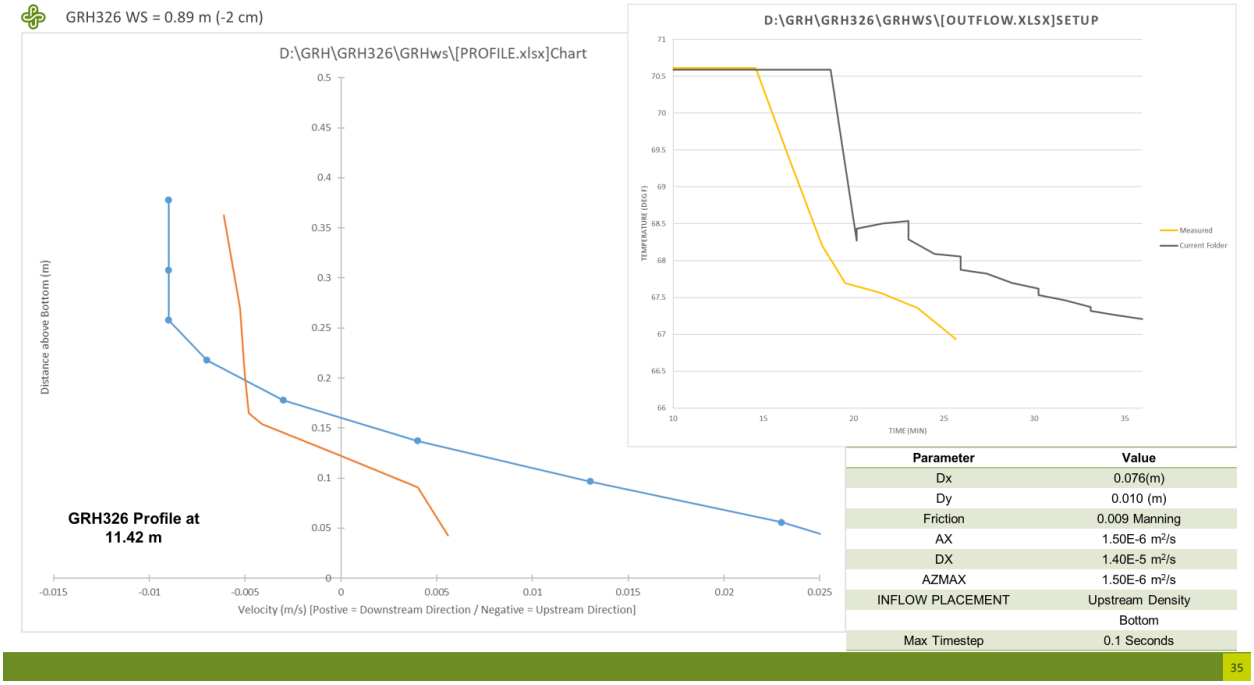

Figure 27: GRH 326 low water surface model results.